

A Bayesian approach to comparing theoretic models to observational data: A case study from solar flare physics

S. Adamakis¹

C. L. Raftery²

R. W. Walsh¹

P. T. Gallagher²

sadamakis@uclan.ac.uk

ABSTRACT

Solar flares are large-scale releases of energy in the solar atmosphere, which are characterized by rapid changes in the hydrodynamic properties of plasma from the photosphere to the corona. Solar physicists have typically attempted to understand these complex events using a combination of theoretical models and observational data. From a statistical perspective, there are many challenges associated with making accurate and statistically significant comparisons between theory and observations, due primarily to the large number of free parameters associated with physical models. This class of ill-posed statistical problem is ideally suited to Bayesian methods. In this paper, the solar flare studied by Raftery et al. (2009) is reanalysed using a Bayesian framework. This enables us to study the evolution of the flare’s temperature, emission measure and energy loss in a statistically self-consistent manner. The Bayesian-based techniques confirm that both conductive and non-thermal beam heating play important roles in heating the flare plasma during the impulsive phase of this event.

Subject headings: Sun: corona — Sun: flares — methods: statistical

1. Introduction

Solar flares are triggered by the instability of the magnetic field. This can result in the direct or indirect heating of chromospheric plasma leading to the process known as “chromospheric evaporation” (Milligan et al. 2006a,b). There are two ways to provoke evaporation (chromospheric

¹Jeremiah Horrocks Institute for Astrophysics and Supercomputing, University of Central Lancashire, Preston, PR1 2HE, UK

²Astrophysics Research Group, School of Physics, Trinity College, Dublin, Dublin 2, Ireland

plasma upflow): using thermal energy and/or using non-thermal energy according to the energy release mechanisms (Mariska et al. 1993). In the thermal energy model, heat is unleashed in the coronal portion of the loop (possibly because of magnetic reconnection). Then the thermal energy is carried downward to the upper chromosphere via conduction, where the deposited energy heats the plasma and stimulates it to move slowly upward. In the non-thermal energy model, the energy release (again in the corona) is in the form of a non-thermal electron beam. Electrons then collide with dense chromospheric plasma, which they heat, causing the plasma to expand both upward at very high speeds and downward at lower speeds.

This paper will focus on the statistical analysis of the observations outlined in Raftery et al. (2009) and will be compared with results from the Enthalpy Based Thermal Evolution of Loops (EBTEL) model (Klimchuk et al. 2008). Comparing to Raftery et al. (2009) this research will handle the statistics with care to derive which of the thermal or non-thermal heat flux is more dominant, during a single flare event, using model comparison techniques (Kass 1993; Kass & Greenhouse 1989; Kass & Raftery 1995; Raftery 1996; Clyde et al. 2007; Adamakis et al. 2008). Furthermore, the method used here treats the uncertainties for the time constraints with equal respect as the uncertainties of the temperature and emission measure, which are difficult to incorporate into our analysis regarding Classical statistics. The thermal heat flux is proportional to the non-thermal heat flux plus a constant background heat flux. The parameter space is extended with the addition of the radius of the loop in order to make the model more realistic. Last but not least, the ratios between the radiative loss rate of the transition and the corona, the average coronal and apex temperature, and the coronal base and apex temperature are assumed to be free parameters so that their values will be decided by the data. For more information about these parameters refer to Section 3.

One advantage of the EBTEL model is that we can incorporate both a direct and a non-thermal heat input, which is not restricted by the data. Thus, in order to produce a temperature and/or density profile, we must assume a specific form for the non-thermal heat flux function. Hence, it is important to understand and evaluate the impact any changes in the thermal and non-thermal heat flux has on the plasma evolution. Several forms of thermal heat fluxes have been tested in Adamakis (2009). Here we present only two of them: Half Gaussian profile and Full Gaussian profile. The rest of the paper has been structured as follows: Section 2 comments on the Raftery et al. (2009) observations and some assumptions in the EBTEL model. Section 3 discusses the details of the analysis regarding the data distribution and the parameter space. Section 4 addresses to the choice of the parameters in the prior distributions. Section 6 presents results of different models and parameter estimations. Finally, Section 7 summarise our findings and presents how this work can be further progressed.

2. Previous Work

2.1. Observations of a C-Class Solar Flare

The temporal evolution of temperature and emission measure in a C3.0 solar flare observed on March 26, 2002 has been analysed. During a typical solar flare, the temperature rises from less than one MK up to ~ 20 MK, and then cools down to the pre-flare temperatures. In the example under consideration here, Raftery et al. (2009) used different instruments to track this evolution: the Reuven Ramaty High Energy Solar Spectroscopic Imager (RHESSI; > 5 MK), GOES-12 (5 – 30 MK), the Transition Region and Coronal Explorer (TRACE 171 Å ; 1 MK), and the Coronal Diagnostic Spectrometer (CDS; $\sim 0.03 - 8$ MK). We note here that TRACE data were not included in the emission measure analysis. This is as a result of the instrument being sensitive to multiple emission lines, making it complex to define the contribution function. The reader is referred to Raftery et al. (2009) which outlines the reasons why and at which particular time of the flare each particular instrument was employed.

The flare began with evidence of pre-flare heating at its onset. This was followed by explosive chromospheric evaporation during the impulsive phase and gentle chromospheric evaporation during the early decay phase. It is believed that the plasma reached a peak temperature of just more than 13 MK in approximately 10 min. Conduction losses dominated over radiative losses for the initial ~ 300 s of the post-flare decay, whereas for the next ~ 4000 s, radiative losses prevailed. Raftery et al. (2009) concluded that approximately equal direct and non-thermal heating mechanisms produced the data observed according only to an estimation of the ratio between the thermal and non-thermal heating rate, which is of course very critical. The best fit and parameter intervals were derived using an acceptable fit to the data by eye.

2.2. The EBTEL Model

The Enthalpy-Based Thermal Evolution of Loops (EBTEL) model (Klimchuk et al. 2008) is a zero-dimensional hydrodynamic (0D HD) model that takes into account the significance of introducing the enthalpy into the system. The difference with the 1D HD model is that the 1D HD model provides us with temperature, density, and velocity profiles along a given magnetic field line as time evolves (that is temperature, density, and velocity are a function of both space and time), whereas 0D HD models describe the average evolution of these values along a coronal strand as a function of time only. Subsequently, 0D HD models require less computing time than 1D models, but at the expense of losing the spatial resolution. In spite of this, the EBTEL code has been used in a wide range of studies regarding different heat input forms (see Klimchuk et al. 2008, for more details). The importance of 0D models compared to the 1D models is that they can give similar results for the plasma response to a sudden heat input, despite the fact that they use up to four orders of magnitude less computing time.

To reflect the physical processes taking place within the standard flare model, the EBTEL model allows for both thermal and non-thermal heating of the plasma in the system. It has been noted that proton precipitation is not included (see Aschwanden 2005). Proton beams are expected to excite strong kinetic Alfvén waves. The turbulence caused by kinetic Alfvén waves contains enough energy to produce the non-thermal velocities observed in flares, and therefore could contribute to impulsive primary plasma heating between the reconnection regions and the flare footpoints.

Deviations of the observations from the model could be caused by two distinct reasons: First, the EBTEL model treats the effects of the non-thermal electron beam in a very simple way. It is assumed that all the beam’s energy goes into evaporating plasma upwards into the loop, which is reasonable for gentle evaporation. However, for explosive evaporation, some of the beam energy will be used to drive chromospheric downflows, making the total observed non-thermal energy larger than that predicted by the EBTEL model. Second, the flare loop is almost certainly constructed of many strands that are heated at different times. Raftery et al. (2009) assume the flaring loop consists of individual strands, all heated simultaneously. Therefore they model the loop as one “fat strand”. However, some strands are likely to be heated at a different time compared to this solid structure.

3. Defining the Model Parameters

3.1. Data Distribution

The errors in temperature come from the width of the contribution function for the particular emission line (for the CDS points) and from the width of the instrument response function for GOES and TRACE. The RHESSI temperature error comes from the uncertainty in the fit to the Maxwell Boltzmann distribution.

As there is no information about the form of the errors, it is assumed that the errors between the observed temperatures and emission measures and those predicted from the model are normally distributed with mean zero and standard deviation derived from the error bars (we assume “ 3σ ” belief; see Adamakis et al. 2008). This means that the likelihood will be of the form:

$$p(\mathbf{D}|\mathbf{P}) = \frac{1}{(2\pi)^{(n_1+n_2)/2} (\prod_{i=1}^{n_1} \sigma_{i1}) (\prod_{i=1}^{n_2} \sigma_{i2})} \exp \left[-\sum_{i=1}^{n_1} \frac{(T_i - \widehat{T}_i(\mathbf{P}))^2}{2\sigma_{i1}^2} - \sum_{i=1}^{n_2} \frac{(EM_i - \widehat{EM}_i(\mathbf{P}))^2}{2\sigma_{i2}^2} \right] \mathcal{I}(\max T < 3 \times 10^7),$$

where $\mathbf{D} = (\mathbf{T}, \mathbf{EM})$ with $\mathbf{T} = (T_1, \dots, T_{n_1})$ the temperature data-points and $\mathbf{EM} = (EM_1, \dots, EM_{n_2})$ the emission measure data-points, \widehat{T}_i and \widehat{EM}_i are the temperatures and emission measures respec-

tively proposed by the EBTEL model, \mathbf{P} is the parameter space (see end of Section 3), n_1 is the number of observed temperature values, n_2 is the number of observed emission measure values, σ_{i1} are the standard deviations of the temperature errors, σ_{i2} are the standard deviations of the emission measure errors and $\mathcal{I}(\cdot)$ is the indicator function which is given by:

$$\mathcal{I}(\max T < 3 \times 10^7) = \begin{cases} 1, & \text{if } \max T < 3 \times 10^7 \text{ K} \\ 0, & \text{otherwise.} \end{cases}$$

where $\max T$ is the maximum temperature value of the cooling curve. The temperature profile is restricted to not exceed 30 MK because it is believed that temperatures above this threshold will create unphysical data.

3.2. Parameters for Non-Thermal Heat Flux

As discussed in Section 1, one of our aims is to compare which of the Half Gaussian and Full Gaussian functions for the non-thermal heat flux fits better to the data observed. In the case of the Half Gaussian the non-thermal heat flux function is given by the form:

$$\mathcal{F}(t) = \begin{cases} \frac{\mathcal{A}}{\sqrt{2\pi}\sigma_1} \exp\left[-\frac{(t-\mu)^2}{2\sigma_1^2}\right], & t \leq \mu \\ 0, & t > \mu \end{cases}$$

where t is the time, μ is the time that maximise the non-thermal heat flux function (which can be adopted as a parameter), σ_1 is a value that defines the width of this distribution (which can be adopted as a parameter as well) and \mathcal{A} is the amplitude of the function (parameter). For the total non-thermal heat function \mathcal{F}_{tot} we have:

$$\mathcal{F}_{tot} = \int_0^\infty \mathcal{F}(t) dt = \int_0^\mu \mathcal{F}(t) dt = P(0 \leq t \leq \mu) \mathcal{A},$$

where $P(\cdot)$ defines the probability. We have $P(0 < t < \mu) = p \leq 0.5$ if and only if $\sigma_1 = \frac{\mu}{\Phi^{-1}\left[\frac{1+2p}{2}\right]}$, where $\Phi^{-1}(\cdot)$ is the cumulative distribution function of the Gaussian distribution with mean 0 and standard deviation 1. In the case that μ is big and σ_1 is small (*e.g.* $\sigma_1 \leq \mu/3$), then $P(0 \leq t \leq \mu) \approx \frac{1}{2}$. For these examples, we can assume $\mathcal{F}_{tot} = \frac{\mathcal{A}}{2}$. Moreover, if \mathcal{F}'_{tot} is the dimensionless total non-thermal heat flux, then $\mathcal{F}_{tot} = \mathcal{F}'_{tot} \times 10^9 \text{ ergs cm}^{-2}$.

In the case of the Full Gaussian the heat flux function is given by the form:

$$\mathcal{F}(t) = \frac{\mathcal{A}}{\sqrt{2\pi}\sigma_1} \exp\left[-\frac{(t-\mu)^2}{2\sigma_1^2}\right].$$

We have $P(t > 0) = p$ (with $0.5 < p \leq 1$) if and only if $\sigma_1 = \frac{\mu}{\Phi^{-1}(p)}$. If again, *e.g.*, $\sigma_1 \leq \mu/5$, then $P(t > 0) \approx 1$ and for these cases we can assume $\mathcal{F}_{tot} = \mathcal{A}$.

3.3. Parameters with the EBTEL Model

The thermal heating rate is assumed to be of the form:

$$Q(t) = \alpha \mathcal{F}_1(t) + B. \quad (1)$$

Here Q is the direct heating rate; $B = B' \times 10^{-5}$ ergs cm $^{-3}$ s $^{-1}$ is a constant background heating rate that is occurring (B' is dimensionless and is included as a parameter); $\mathcal{F}_1(t)$ is the non-thermal heating rate with $\mathcal{F}_1(t) = \frac{\mathcal{F}(t)}{L}$ where $L = L' \times 10^9$ cm is the loop's length from the top of the chromosphere to the apex (parameter); and α is a factor that defines which of the two heating functions (thermal or non-thermal) is dominant assuming that the background heating rate is negligible comparing the other two heating sources. Under this assumption, if $\alpha = 1$ we have equal amounts of thermal and non-thermal heating, if $\alpha > 1$ then thermal heat flux is more dominant, whereas if $\alpha < 1$ then non-thermal heat flux is more dominant. In particular, we will be examining comparisons of the form: $H_0 : \alpha \neq 1$, $H_1 : \alpha = 1$, $H_2 : \alpha > 1$ and $H_3 : \alpha < 1$. Finally, we include the dimensionless radius of the loop r' (assuming the loop to be homogeneous), with $r = r' \times 10^9$ cm, as another parameter into our analysis. The importance of r' is that we calculate $2n_e^2\pi r^2 L$ in order to compare it with the observed emission measure values.

There has been much debate about the parameters $c_i, i = 1, \dots, 3$ in the Klimchuk et al. (2008) paper, where $c_1 = \frac{R_{tr}}{R_c}$ is the ratio of the radiative loss function between the transition region and the corona, $c_2 = \frac{\bar{T}}{T_a}$ the ratio between the average temperature at the coronal part of the loop and the temperature at the apex of the loop and $c_3 = \frac{T_0}{T_a}$ is the ratio between the temperature at the base of the corona and the temperature at the apex of the loop. In Section 6.1, these values are assumed to be fixed to given numbers, whereas in Section 6.2 they are assumed to be free parameters which can be determined by the data.

3.4. Dealing with time

The data values have uncertainties (error bars) not only on the y axis (temperature and emission measure), but also on the x axis (time). These time errors were calculated as being the width of the spline interpolated light curves. There have been some attempts in the past to deal with problems of error bars in both axes (Winsor 1946; Berkson 1950; Jaynes 1991). A Bayesian solution to the problem using the reversible jump MCMC algorithm can be found in Henderson et al. (2000). According to this, the *true* time¹ should be included as another parameter.

¹In statistics, the *true* value of a variable (e.g. T_{true}) is based on the *observed* value of that variable (T_{obs}) with the addition of an error (ΔT), i.e. $T_{true} = T_{obs} + \Delta T$.

All in all, the parameter space would be: $\mathbf{P} = (\mathbf{P}_1, \mathbf{P}_2)$, with $\mathbf{P}_1 = (t_1, \dots, t_{n_1})$, where t_i is the time for the i th observation, and $\mathbf{P}_2 = (L', \mathcal{F}'_{tot}, \mu, \sigma_1, \alpha, B', r')$ for Section 6.1 and $\mathbf{P}_2 = (L', \mathcal{F}'_{tot}, \mu, \sigma_1, \alpha, B', r', c_1, c_2, c_3)$ for Section 6.2.

4. Defining the Priors for the Parameters

There is a very important difference between Classical statistics and Bayesian statistics. The former does not consider any prior information for the parameters, whereas the latter can incorporate any information we have about the parameters before we observe the data. Further discussion on choosing priors can be found in Kass & Wasserman (1996), while the importance of priors in model comparison can be found in Kass (1993), Kass & Greenhouse (1989) and Adamakis (2009).

Thus, prior distributions are constructed based on our prior knowledge about where the parameters should lie. Non-informative priors are employed where we do not have any prior information at all. The belief we have *before* we undertake the analysis in Section 6 is summarised in Table 1. From the observations we conclude that L' should be around 3 and probably between 2 and 4. We have the option to give more weight to the value of 3 and less weight as we move away from that value. Hence, we assume that $L' \sim \mathcal{G}(37.64, 0.08)$ which will give a 95% probability between 2 and 4 with mode at 3. For the total non-thermal energy \mathcal{F}'_{tot} we do not have any information at all, therefore $\mathcal{F}'_{tot} \propto 1$.

We assume that the flare observations are from the cooling phase of the temperature profile; from the highest temperature lines downwards, the temperature drops continually. Thus, it is very likely that the main flare energy release will occur at most up until the first observation. For this reason we choose the mean of the non-thermal heat flux (μ) to have an upper limit at the lower error bar of the first observation (which is 884 s after the beginning of the observational period). Since we do not have any other belief about giving weights to any specific values we assume $\mu \propto \mathcal{I}(\mu \leq 884)$, where $\mathcal{I}(\cdot)$ is the indicator function (see Section 3.1). Also, $\sigma_1 \sim \mathcal{G}(6.78, 17.28)$ will give 95% probability for the one standard deviation of the heating function to be between 20 and 200 with mode at 100. Since we do not have any knowledge about the background heating, we can assume an improper prior, *e.g.* $\pi(B') \propto 1$. In Section 6.2 we use $\mathcal{G}(1.70, 2.36)$ as a prior for c_1 and $\mathcal{U}(0, 1)$ prior for c_2, c_3 . The prior for c_1 will give $\sim 99.90\%$ probability for values below 20 and those for c_2 and c_3 come naturally as they will impose an upper limit of one, without favouring any values below unity. Note that the prior for c_2 can be conservative, as there might be evidence that this number is close to the value 0.87 (Klimchuk et al. 2008).

For the radius of the loop as observed in Figure 1 from Raftery et al. (2009), we assume that the ratio $R = \frac{r'}{L'}$ is probably 1/6. It is certainly no more than 1/2; so we give the ratio a 99.73% probability to be inside the interval [0, 0.5]. For this reason we have $R \sim \mathcal{G}(6.03, 0.03)$. Since $r' = R \times L'$ and R, L' have known prior distributions, we can simulate the prior distribution of r' to be $\mathcal{G}(5.23, 0.12)$, which will give 95% probability between [0.20, 1.24] with mode at 0.49.

Since we do not have any prior information regarding the α parameter, it would be preferable to give it an uninformative prior just as with B' . However, the fact that it is the “important” parameter of the analysis (if we want to test the hypotheses $H_i, i = 0, \dots, 3$) it has been given an informative prior, otherwise this would lead to Bartlett’s paradox (Lindley 1957; Bartlett 1957). Thus, a probability density function that will give a 50% probability for $\alpha < 1$ and a 50% probability for $\alpha > 1$ was chosen. For the H_0 hypothesis ($\alpha \neq 1$), this probability density function will be of the form:

$$\pi(\alpha) = \begin{cases} 0.5, & 0 < \alpha < 1 \\ 0.5 \exp(1 - \alpha), & \alpha > 1; \end{cases}$$

for the H_2 hypothesis ($\alpha > 1$), $\pi(\alpha) = \exp(1 - \alpha)$; and for the H_3 hypothesis ($\alpha < 1$), $\alpha \sim \mathcal{U}(0, 1)$. As far as the true time is concerned we can assume that it is normally distributed about the observed time with standard deviation obtained from the time error bars.

Our last assumption involves the initial values of the temperature, density and emission measure. For this, we assume the pre-flare conditions to have an upper limit of 0.5 MK, $6 \times 10^7 \text{ cm}^{-3}$ and $4 \times 10^{43} \text{ cm}^{-3}$ respectively (Raftery et al. 2009). Since the non-thermal heating rate is almost zero in the beginning, then because of Equation (1), the dominant heat input will be the background heating rate. Hence, these upper limits can indirectly serve as an upper limit to the background heating rate.

5. Model Comparison Methods

Model comparison methods using Bayesian statistics are reviewed in great detail in Clyde et al. (2007). An excellent description of how Bayes factor is applied in several problems can be found in Kass & Raftery (1995) and Raftery (1996). The key value for estimating the Bayes factor is to calculate the marginal density function:

$$p(\mathbf{D}|H_k) = \int_{\mathbf{P}} p(\mathbf{D}|\mathbf{P})\pi(\mathbf{P})d\mathbf{P},$$

where H_k is the hypothesis (model) under consideration, $p(\mathbf{D}|\mathbf{P})$ is the likelihood function and $\pi(\mathbf{P})$ is the prior distribution. Basically, the marginal distribution is nothing more than the belief that we have about the data after we have integrated all the parameters, for the specific model under consideration. Then, the Bayes factor is given by:

$$BF_{01} = \frac{p(\mathbf{D}|H_0)}{p(\mathbf{D}|H_1)}, \quad (2)$$

for testing two hypotheses (H_0 and H_1). From Equation (2) it is clear that if $BF_{01} \gg 1$ there is more evidence in favour the H_0 hypothesis, if $BF_{01} \ll 1$ there is more evidence in favour the H_1 hypothesis, whereas if $BF_{01} \approx 1$ the data do not favour either model (but see Kass & Raftery 1995, for more information). Thus, the challenge here is to calculate the marginal densities. Since

they are very difficult to calculate analytically, we will turn to numerical methods. In this paper we employ the two-stage sampler described in Adamakis et al. (2008).

We also employ the Akaike Information Criterion (AIC), proposed by Akaike (1974), and the Bayesian Information Criterion (BIC), proposed by Schwarz (1978). AIC propose to choose the model that minimises:

$$\text{AIC} = -2(\log \text{maximised likelihood}) + 2\lambda,$$

whereas the latter chooses the model that minimises:

$$\text{BIC} = -2(\log \text{maximised likelihood}) + \lambda \log n,$$

where λ is the number of the parameters and n is the number of the data-points.

6. Results

The analysis can be separated into three crucial questions:

1. Which of the Half Gaussian and Full Gaussian functions fits better to the data we have?
2. Which of the thermal and non-thermal heat fluxes is dominant?
3. Should the c_i values remain fixed or should they be free parameters?

The second question is the most important regarding the physics of the system. The other two questions are associated more with the statistical analysis. Nevertheless, they can indirectly affect which heat flux is most dominant because they contain relevant parameters. The estimations of the marginal densities of the different models that are shown in Figure 1 are presented in Table 2. For all the statistical models we have assumed that the mean energy of the accelerated (non-thermal) electrons impinging the chromosphere is $\mathcal{E} = 15$ keV. Different values of \mathcal{E} do not have a large effect on the temporal profiles.

Since we do not have any prior information for the α parameter and we have decided to give an informative prior distribution in order to avoid Bartlett’s paradox, we have undertaken the same analysis with a non-informative prior for α . The reason for this is because we wanted to check the sensitivity of the analysis regarding the prior restriction of the α parameter. Thus, we use the results obtained from Table 2 with non-informative prior for α to approach Questions 1 and 3 and the results obtained with informative priors for α to decide which heating mechanism (thermal or non-thermal) prevails.

6.1. c_i Fixed

6.1.1. Model selection

The c_i parameters are fixed at $c_1 = 4, c_2 = 0.87, c_3 = 0.72$ due to an acceptable overall agreement with 1D HD simulations (Raftery et al. 2009; Klimchuk et al. 2008). From Table 2 and with a non-informative prior for α we can derive that the Bayes factor between the Full Gaussian and the Half Gaussian heating function is 42.10 using the Importance sampling estimator. This provides “strong” evidence in favour of the Full Gaussian, according to the table in Kass & Raftery (1995). By looking the results for the $H_0 : \alpha \neq 1$ hypothesis, there is “positive” evidence in favour of the Full Gaussian. The information criteria agree with this conjecture (see Table 3). Note that the values for AIC and BIC are the same for the hypotheses $\alpha \neq 1$ because the information criteria do not depend on the priors. From this, we can conclude that there is enough evidence to support that the Full Gaussian function for the heating profiles is much more adequate than the Half Gaussian, at least for the particular data-set under analysis.

In order to distinguish between the thermal and non-thermal heat fluxes, let us focus on the results from Table 2 with the informative prior for α . Roughly speaking, the model with the largest marginal density will provide evidence of its favour among a given class of models. Using the Full Gaussian we conclude that the evidence we get is “not worth more than a bare mention” for any hypothesis ($\alpha > 1, \alpha < 1, \alpha = 1$). We reach the same conclusion for the Half Gaussian as all the marginal probability densities are almost the same. On the other hand the information criteria select the $\alpha = 1$ hypothesis for both Gaussian functions. This time, the model that minimises the information criteria can be proven more useful among a given set of models.

Thus, if we had to choose one of the three hypotheses, we would have chosen $\alpha = 1$, *i.e.* equal amount of thermal and non-thermal heat input, as there is lack of evidence to support a more complicated statistical model. Since the Full Gaussian is more preferable than the Half Gaussian we will choose to adopt the Full Gaussian results for estimating the parameters.

6.1.2. Parameter estimation

The results of this analysis with non-informative prior for α can be viewed in Table 4. We estimate the mean of L to be 29.20 Mm, which is close to what was used by Raftery et al. (2009) (*i.e.* 30 Mm). The mean total non-thermal heat flux is calculated around 79.83×10^9 ergs cm^{-2} , while mean time for the peak of this function is 853.5 s after the beginning of the flare. For the α parameter a 95% credible interval gives [1.30, 101.30], whereas the probability $P(\alpha > 1) = 55.86\%$ with informative prior for α . We expected the posterior probability of $\alpha > 1$ to be close to 1/2, as the Bayes factor could not provide enough evidence in favour of the hypotheses $\alpha > 1$ or $\alpha < 1$ (Table 2). An interesting point to note here is that if we use non-informative prior for α , we can conclude that since $\hat{\alpha} = 20.90$ then the $\alpha > 1$ hypothesis is preferable. This is of course something

that is misused in astrophysics and can lead to false conclusions. More discussion about this is presented in Section 7.

The first column of Figure 2 shows the best fit of the parameters regarding the posterior distributions. Even by eye we can distinguish between the Full Gaussian and the Half Gaussian function. As previously discussed, introducing a prior distribution for the α parameter, while there is no prior information, will create a bias. This is the price we have to pay in order to address Question 2. However, the prior we employed seems reasonable as it provides 1/2 probability for $0 < \alpha < 1$ and, subsequently, 1/2 probability for $\alpha > 1$. In order to see how different the results are, both with and without prior information for the α parameter, then we compare Table 4 with the respective table we get from the analysis where prior information for α is imported. From that we can conclude that all the parameters have almost the same posterior distributions, apart from the \mathcal{F}_{tot} parameter. Especially for this parameter, a 95% highest posterior density interval² will give [51.51, 544.56] with informative prior for α and [2.11, 171.90] with non-informative prior for α .

6.2. c_i Parameters

6.2.1. Model selection

We follow the same procedure as in Section 6.1.1 in order to derive the models that best describe the data. Regarding which of the two non-thermal heat fluxes is more dominant, there is no question that the Full Gaussian is more preferable as can be seen from Table 2 (the Bayes factor in favour of the Full Gaussian is 142.54 with non-informative prior for α , according to the Importance sampling estimator). This can be characterised as “very strong” evidence in favour of the Full Gaussian. The same preference for the Full Gaussian function can be derived by comparing the log-marginal densities for $\alpha \neq 1$ with informative prior for α . From Table 3 the information criteria are in agreement with this. Therefore, the fact that we included the c_i as free parameters, did not alter the outcome comparing to the analysis in Section 6.1.1 where the c_i are fixed.

Using an informative prior for α and the Full Gaussian non-thermal heat flux, it can be concluded from Table 2 that the $\alpha > 1$ hypothesis is slightly better than the other two. But this evidence is not that strong and it can be characterised as “not worth more than a bare mention”. For the Half Gaussian model the same picture is obtained: the data we have cannot distinguish which of the thermal or non-thermal heat fluxes is more dominant, if either. The information criteria (see Table 3) choose the Full Gaussian distribution and $\alpha = 1$. Therefore, if we had to choose a hypothesis we would go for equal amount of thermal and non-thermal heat flux ($\alpha = 1$).

²A 95% highest posterior density interval of a parameter leaves 95% probability for the parameter to be inside this credible interval and any value of the posterior distribution that is inside this credible interval is higher than any value of the posterior distribution that is outside this credible interval (Carlin & Louis 2000; Chen et al. 2000; Aitken & Taroni 2004).

6.2.2. Parameter estimation

All the estimations from the posterior distributions of the parameters can be viewed in Table 4, using the Full Gaussian function. We estimate the mean of L to be 31.6 Mm, the mean of the total non-thermal heat flux is 31.99×10^9 ergs cm^{-2} , the mean time for the peak of this function 864.6 s after the beginning of the flare, the mean of the standard deviation of the Full Gaussian is 92.6 s, the mean of the α parameter is 23.51, the mean background heating rate is 0.12×10^{-5} ergs $\text{cm}^{-3} \text{ s}^{-1}$ and the radius of the loop is 6.7 Mm.

Regarding the c_i ratios, the mean of the ratio between the radiative loss rate of the transition and the corona (c_1) is 2.07, the mean of the ratio between the average coronal temperature and the apex temperature (c_2) is 0.86 and the mean of the ratio between the coronal base temperature and the apex temperature (c_3) is 0.75. Once again, we should bear in mind that although the estimation for α is greater than unity (23.51) with non-informative prior, a more detailed analysis shown in Section 6.2.1 suggests that we cannot distinguish which of the thermal or non-thermal heat fluxes is more dominant. Furthermore, assuming informative prior for α , α is greater than unity with probability 57.13%. The second column of Figure 2 shows the best fit of the parameters regarding the posterior distributions for both the Full and Half Gaussian functions.

As in Section 6.1.2, we want to check the sensitivity of the analysis regarding the prior information for α . Comparing Table 4 with the respective table we get when we use informative prior for α , then the only difference worth mentioning is the \mathcal{F}'_{tot} parameter which will give a 95% highest posterior density interval [37.33, 318.38] for informative prior for α and [3.26, 119.65] for non-informative prior for α .

6.3. Comparison Between the Hypotheses: c_i Fixed and c_i Free Parameters.

Considering the non-thermal heat flux, both of the two hypotheses (c_i fixed and c_i free parameters) propose the Full Gaussian statistical model. However, none of them can distinguish which of the two heating mechanisms is dominant (if any). Regarding Question 3, from Table 2 we reach different conclusions depending on the estimation method for the marginal distribution: Importance sampling do not seem to favour any hypothesis, but the other two methods favour the hypothesis c_i free parameters. However, the information criteria (Table 3) clearly choose the hypothesis c_i free parameters. This indicates that the values introduced for c_i when they are fixed are not very good, in terms of maximising the likelihood function. The information added when c_i are free parameters is higher than the price we have to pay for introducing three additional parameters.

Figure 3 provides a graphical representation of the hypotheses: c_i fixed and c_i free parameters. The difference does not seem to be very important for the thermal evolution (first row), at least by eye. However, for the data-set under consideration, the difference is more profound for the emission measure evolution (second row). This indicates that the c_i parameters affect more the emission

measure values than the temperature values. The fact that there are better values for c_i than 4, 0.87 and 0.72 is even more clear in the third row where temperature is plotted against emission measure.

7. Discussion

In order to reveal the mysteries of the Sun, we can break down our investigations into three major stages: (*i*) constructing theoretical models, (*ii*) gathering observations, and (*iii*) applying a statistical analysis in order to compare different statistical models and/or to restrict the parameters of the models. All of them are of equal importance and give us confidence in our results.

Making inference alone from the mean or mode of Table 4 is of utmost criticism. For model comparison purposes the 95% credible interval is more robust. However, even with the 95% credible interval we can not compare with the $\alpha = 1$ hypothesis. Also, we do not directly include the likelihood function in our calculations. On the other hand, model comparison techniques like AIC and BIC take into account the likelihood function but ignore the spread of the parameter distributions. However, model comparison techniques using Bayesian statistics (*e.g.* Bayes factor) take into account both the spread of the parameter posterior distributions and the information of the likelihood function.

In this paper, temperature and emission measure profiles produced by the EBTEL model were compared with solar flare observations. The data distribution, the parameter space and the priors employed in this analysis were described in great detail. The form of thermal and non-thermal heat input is much better described using Full Gaussian energy profile than Half Gaussian, which is what Raftery et al. (2009) also used. This is not surprising as the heating function is expected to mimic the X-ray profile, which is often found to be Gaussian-like.

Apart from choosing which function was more appropriate for the data-set we analysed, we were also interested in determining which of the thermal or non-thermal heat fluxes was more dominant. The data obtained were not able to provide an answer with great confidence. More data-points may be required in order to address this question. However, this result implies that both thermal and non-thermal heating mechanisms are almost equally important during the flaring process. Although, this is in agreement with Raftery et al. (2009), we fully recommend a proper treatment of statistics as we may be led to fallacious results as in Ugarte-Urra et al. (2005), which were discovered in Adamakis et al. (2008).

The c_i parameters were given fixed values in the Klimchuk et al. (2008) paper so that the 0D HD model will approximate the 1D HD model. If we assume that the range of these parameters provides sufficient approximations, then we should include them as free parameters. In any case, we disagree with fixing some parameters to certain values, in order to reduce the parameter space, as this might affect the results — unless we have high confidence about these fixed numbers.

The fact that the Bayes factor is not so decisive in choosing between the hypotheses c_i fixed or free parameters is partially an outcome of the conservative prior distributions we have chosen for the c_i parameters (see Section 4). If we had added more information in the prior distribution of c_2 , say $\mathcal{U}(0.5, 1)$ or even better the Beta distribution $\mathcal{B}(38.49, 5.75)$, this would have been in favour of the c_i parameters hypothesis. However, since we do not know anything about these values in advance, it is better to have them as free parameters and let the simulation decide upon these values. More improved estimations for these parameters can be seen from the mean or mode of Table 4 (for the particular data-set we analyse).

Finally, an obstacle presented in this analysis was that of constraining the profiles produced by the EBTEL model. For example, we might not want to restrict the initial values of temperature, density and/or emission measure profiles. This might produce model profiles that are closer to the data profiles, but the initial values might take exceptionally high numbers. For example, we had undertaken the same analysis without fixing the initial values of temperature, density and emission measure. This resulted in model profiles with initial temperatures of 3 MK, initial electron density of $500 \times 10^7 \text{ cm}^{-3}$ and initial emission measures of $3 \times 10^{47} \text{ cm}^{-3}$. This was because the background heating rate was three orders of magnitude higher than that in Table 4. Apart from unrealistic estimations of the parameters of interest, this could have also have led to unreliable Bayes factor estimations with false conclusions regarding the three posed questions in the beginning of Section 6. Naturally, the quality of the output of the analysis is dependent of the quality of the input.

Apart from improved statistical techniques, of equal importance is that improvement upon the observations should be made. This means that future missions with new instrumentation should provide data-sets with a large enough number of observations in order to distinguish between different heating mechanisms. The data-set under consideration provided information only upon the decay phase of the temporal evolution. However, a better time resolution for the rise phase of the temperature will be needed in order to provide a better estimate for the form of thermal/non-thermal heat flux. And of course, a large sample of solar flares will be required.

An assumption made by Raftery et al. (2009) was that the thermal and non-thermal fluxes have the same form, based on a lack of information on the thermal distribution. However, it would be interesting to test fluxes of different forms that do not depend on each other. Additionally, a further improvement in the EBTEL model is required regarding the non-thermal heat flux, as it is efficient for gentle chromospheric evaporation but suffers from inadequately representing explosive chromospheric evaporation. In addition, several other forms of heating input, like proton beams, could be included in an attempt to make the model more realistic.

SA has been supported by a STFC grant. CLR is supported by an ESA/Prodex grant, administered by Enterprise Ireland.

REFERENCES

- Adamakis, S. 2009, PhD thesis, University of Central Lancashire
- Adamakis, S., Walsh, R., & Morton-Jones, T. 2008, Constraining Coronal Heating: Employing Bayesian Analysis Techniques To Improve the Determination of Solar Atmospheric Plasma Parameters, [arXiv:0807.4209]
- Aitken, C. & Taroni, F. 2004, *Statistics and the Evaluation of Evidence for Forensic Scientists* (John Wiley and Sons Ltd.)
- Akaike, H. 1974, *IEEE Transactions on Automatic Control*, 19, 716
- Aschwanden, M. 2005, *Physics of the Solar Corona: An Introduction with Problems and Solutions* (Springer Praxis Books/Astronomy and Planetary Sciences)
- Bartlett, M. S. 1957, *Biometrika*, 44, 533
- Berkson, J. 1950, *Journal of the American Statistical Association*, 45, 164
- Carlin, B. & Louis, T. 2000, *Bayes and Empirical Methods for Data Analysis* (Chapman and Hall/CRC)
- Chen, M.-H., Shao, Q.-M., & Ibrahim, J. 2000, *Monte Carlo Methods in Bayesian Computation* (Springer-Verlag New York, Inc.)
- Clyde, M., Berger, J., Bullard, F., et al. 2007, in *Statistical Challenges in Modern Astronomy IV*, ed. G. J. Babu & E. D. Feigelson (ASP Conference Series, Vol. 371), 224–240
- Henderson, R., Morton-Jones, A., & McKnespiey, P. 2000, *Applied Statistics*, 49, 563
- Jaynes, E. 1991, *Straight Line Fitting – A Bayesian Solution* [Internet] (Updated 21 April 1999), Technical Report. Available at <http://bayes.wustl.edu/etj/node2.html> [Accessed 22 March 2008]
- Kass, R. E. 1993, *Statistician*, 42, 551
- Kass, R. E. & Greenhouse, J. 1989, *Statistical Science*, 4, 310
- Kass, R. E. & Raftery, A. 1995, *Journal of the American Statistical Association*, 90, 773
- Kass, R. E. & Wasserman, L. 1996, *Journal of the American Statistical Association*, 91, 1343
- Klimchuk, J., Patsourakos, S., & Cargill, P. 2008, *The Astrophysical Journal*, 682, 1351
- Lindley, D. V. 1957, *Biometrika*, 44, 187
- Mariska, J., Doschek, G., & Bentley, R. 1993, *The Astrophysical Journal*, 419, 418

- Milligan, R., Gallagher, P., Mathioudakis, M., et al. 2006a, *The Astrophysical Journal*, 638, L117
- Milligan, R., Gallagher, P., Mathioudakis, M., & Keenan, F. 2006b, *The Astrophysical Journal*, 642, L169
- Raftery, A. E. 1996, in *Markov Chain Monte Carlo in Practice*, ed. W. Gilks, S. Richardson, & D. Spiegelhalter (Chapman and Hall), 163–188
- Raftery, C., Gallagher, P., Milligan, R., & Klimchuk, J. 2009, *Astronomy & Astrophysics*, 494, 1127
- Schwarz, G. 1978, *Annals of Statistics*, 6, 461
- Ugarte-Urra, I., Doyle, J. G., Walsh, R. W., & Madjarska, M. S. 2005, *Astronomy & Astrophysics*, 439, 351
- Winsor, C. 1946, *Biometrics Bulletin*, 2, 101

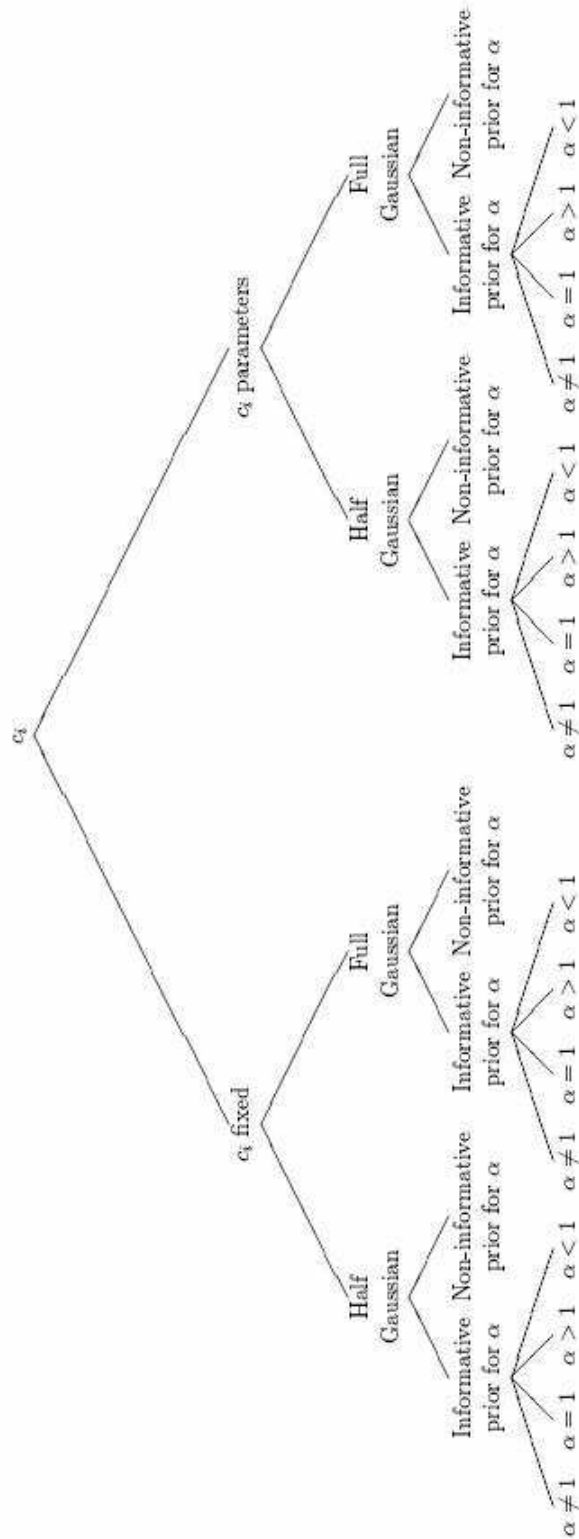


Fig. 1.—: Tree diagram that depicts all the different hypotheses we have used. The purpose of using these hypotheses is to compare them and select the one that best describes the data-set we have.

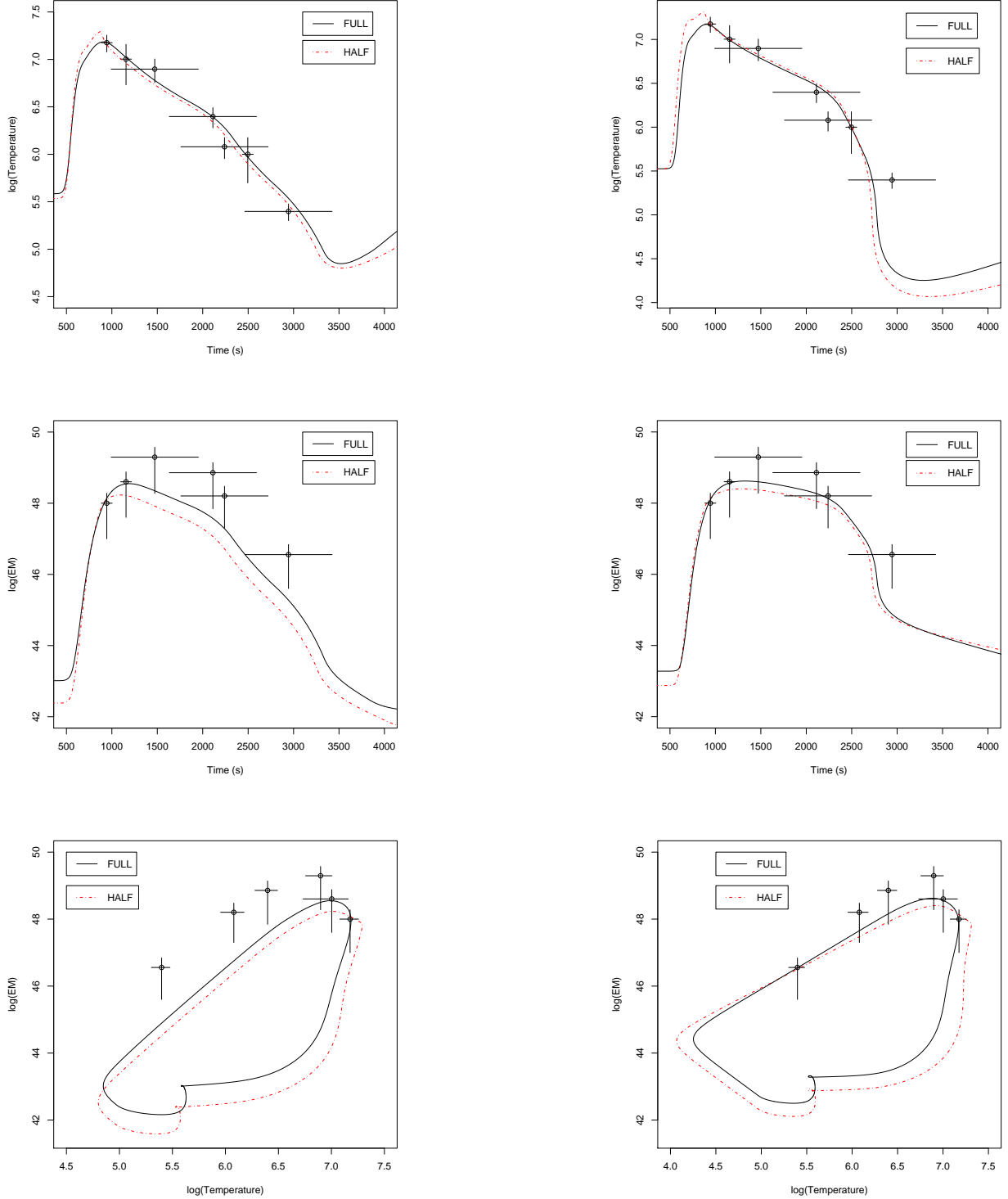


Fig. 2.—: Temperature evolution (*first row*), emission measure evolution (*second row*) and temperature against emission measure (*third row*) using the EBTEL model that best reproduced the observations (maximised the posterior distributions). Solid lines represent the fit from the Full Gaussian function for the thermal and non-thermal heat inputs, whereas dashed lines represent the fit from the Half Gaussian function. For all the curves **non-informative** prior for α was employed. *First column* depicts solutions using the c_i fixed, whereas *second column* depicts solutions from c_i

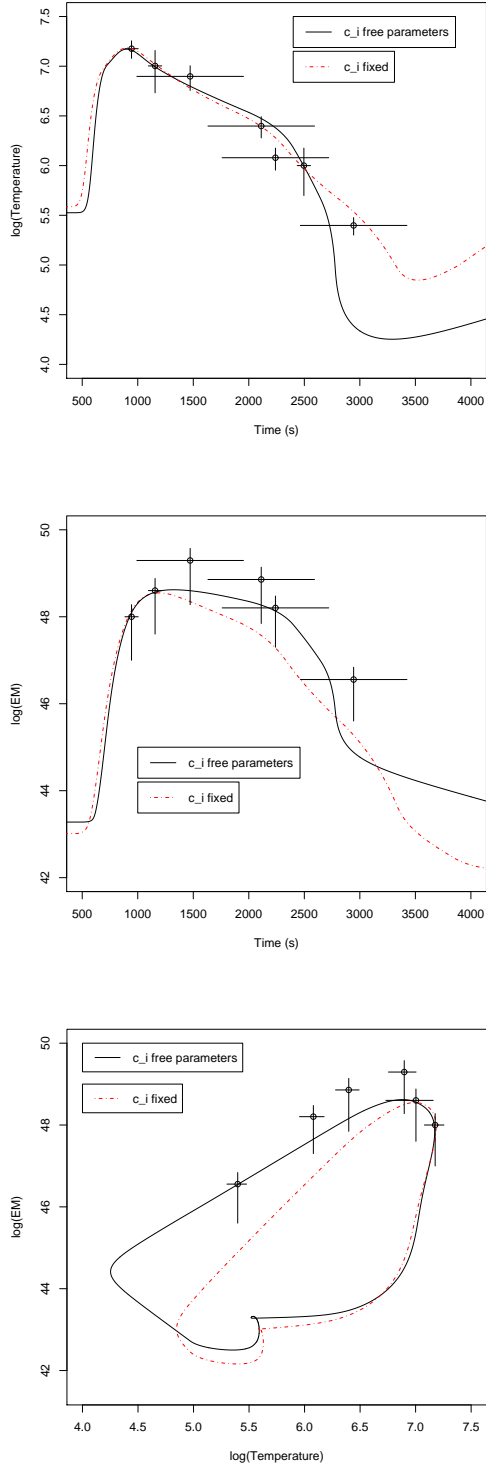


Fig. 3.—: Temperature evolution (*first row*), emission measure evolution (*second row*) and temperature against emission measure (*third row*) using the EBTEL model that best reproduced the observations. Solid lines represent the fit when c_i are floating as free parameters, whereas dashed lines assume c_i to be fixed numbers. Each curve depicts the best fit that maximised the posterior distribution of the Full Gaussian statistical models. **Non-informative** prior for α was employed. Temperature is measured in K, while emission measure is in cm^{-3} .

Table 1:: Prior belief about the parameters.

	mode	95% probability	prior distribution
L'	3	[2,4]	$\mathcal{G}(37.64, 0.08)$
F'_{tot}	NA	NA	$\propto 1$
μ	NA	NA	$\propto \mathcal{I}(\mu \leq 884)$
σ_1	100	[20,200]	$\mathcal{G}(6.78, 17.28)$
α	NA	NA	$\propto 1$
B'	NA	NA	$\propto 1$
r'	0.49	[0.20,1.24]	$\mathcal{G}(5.23, 0.12)$
c_1	NA	NA	$\mathcal{G}(1.70, 2.36)$
c_2	NA	NA	$\mathcal{U}(0, 1)$
c_3	NA	NA	$\mathcal{U}(0, 1)$

Table 2:: Logarithmic marginal densities estimations under several hypotheses, using the EBTEL model to compare with temperature and emission measure profiles (Raftery et al. 2009). This table produces results for both c_i fixed and free parameters for comparison tests. The logarithmic marginal densities are estimated using: 1: Laplace method with posterior covariance matrix, 2: Laplace method with robust posterior covariance matrix, 3: Importance sampling estimation with the probability density from stage 1 as the additional probability density (Adamakis et al. 2008).

				Log-marginal densities		
				1	2	3
c_i fixed	Half Gaussian	Informative prior for α	$\alpha \neq 1$	-796.43	-797.78	-797.66
			$\alpha = 1$	-797.38	-798.19	-797.37
			$\alpha > 1$	-797.20	-798.29	-797.53
			$\alpha < 1$	-797.34	-798.54	-797.99
			Non-informative prior for α	$\alpha \neq 1$	-792.88	-793.68
	Full Gaussian	Informative prior for α	$\alpha \neq 1$	-793.82	-795.28	-794.84
			$\alpha = 1$	-794.45	-795.39	-794.40
			$\alpha > 1$	-793.87	-794.93	-794.42
			$\alpha < 1$	-794.17	-795.31	-794.73
			Non-informative prior for α	$\alpha \neq 1$	-789.07	-790.48
c_i free parameters	Half Gaussian	Informative prior for α	$\alpha \neq 1$	-793.26	-795.98	-798.47
			$\alpha = 1$	-793.36	-796.26	-798.06
			$\alpha > 1$	-794.07	-795.91	-797.96
			$\alpha < 1$	-793.23	-796.60	-797.62
			Non-informative prior for α	$\alpha \neq 1$	-798.65	-792.36
	Full Gaussian	Informative prior for α	$\alpha \neq 1$	-791.06	-793.25	-794.28
			$\alpha = 1$	-790.26	-792.38	-794.39
			$\alpha > 1$	-789.99	-792.37	-794.32
			$\alpha < 1$	-791.48	-793.32	-794.71
			Non-informative prior for α	$\alpha \neq 1$	-786.85	-788.49

Table 3:: Information criteria for comparison between temperature/emission measure profiles produced using the EBTEL model and observations (Raftery et al. 2009). This table produces results for both c_i fixed and free parameters for comparison tests.

				AIC	BIC
c_i fixed	Half Gaussian	Informative prior for α	$\alpha \neq 1$	1590.17	1589.41
			$\alpha = 1$	1587.22	1586.52
			$\alpha > 1$	1590.77	1590.02
			$\alpha < 1$	1590.17	1589.41
	Non-informative prior for α		$\alpha \neq 1$	1590.17	1589.41
	Full Gaussian	Informative prior for α	$\alpha \neq 1$	1582.41	1581.65
			$\alpha = 1$	1581.13	1580.43
			$\alpha > 1$	1582.41	1581.65
$\alpha < 1$			1583.14	1582.38	
Non-informative prior for α		$\alpha \neq 1$	1582.41	1581.65	
c_i free parameters	Half Gaussian	Informative prior for α	$\alpha \neq 1$	1573.52	1572.60
			$\alpha = 1$	1571.88	1571.02
			$\alpha > 1$	1573.52	1572.60
			$\alpha < 1$	1573.98	1573.06
	Non-informative prior for α		$\alpha \neq 1$	1573.52	1572.60
	Full Gaussian	Informative prior for α	$\alpha \neq 1$	1568.76	1567.84
			$\alpha = 1$	1567.62	1566.75
			$\alpha > 1$	1568.76	1567.84
$\alpha < 1$			1569.05	1568.13	
Non-informative prior for α		$\alpha \neq 1$	1568.76	1567.84	

Table 4:: Summary of the posterior inference for both c_i fixed and free parameters with **non-informative** prior for α . Results steam from a Full Gaussian non-thermal heat flux profile.

		mean	mode	s.d.	2.5%	50%	97.5%
c_i fixed	L'	2.92	2.86	0.12	2.69	2.91	3.19
	\mathcal{F}'_{tot}	79.83	44.72	62.96	3.77	75.73	179.88
	μ	853.5	881.1	31.6	763.0	863.8	883.1
	σ_1	101.8	94.2	26.9	54.4	99.6	154.6
	α	20.90	8.46	28.23	1.30	5.74	101.30
	B'	0.19	0.25	0.11	0.01	0.20	0.36
	r'	0.47	0.51	0.12	0.25	0.45	0.73
c_i free parameters	L'	3.16	2.80	0.43	2.43	3.13	4.12
	\mathcal{F}'_{tot}	31.99	8.35	40.11	4.84	13.57	153.98
	μ	864.6	880.6	18.7	813.2	870.3	883.5
	σ_1	92.6	82.0	24.2	51.8	90.5	146.2
	α	23.51	38.09	15.94	1.13	23.48	47.09
	B'	0.12	0.21	0.07	0.01	0.17	0.24
	r'	0.67	0.57	0.17	0.39	0.66	1.05
	c_1	2.07	1.39	0.77	0.81	1.99	3.79
	c_2	0.86	0.88	0.07	0.73	0.87	0.99
	c_3	0.75	0.69	0.13	0.48	0.75	0.98